Article

π-Stacking among the Anthracenyl Groups of a Copper Complex Resulted in Doubling of Unit Cell Volume To Provide New Polymorphs

Abhay Pratap Singh and Jubaraj B. Baruah*

Read Online

ACCESS | Metrics & More | Article Recommendations | SI Supporting Information

ABSTRACT: Two polymorphs of the 9-N-(3-imidazolylpropylamino)methylanthracene (Hanthraimmida) containing hydrated copper(II)-2,6-pyridinedicarboxylate complex are reported. The two polymorphs have either lamellar or Herringbone arrangements of π-stacks among the anthracenyl groups of organocation. The difference between the two polymorphs originated from having face-to-face stacking arrangements between the two anthracenyl groups of the symmetry independent cations within the unit cell in one of the polymorphs. The π-stacked anthracenyl groups in consecutive layers of the polymorphs are oriented in one direction in the polymorph designated as **P1**, whereas the polymorph designated as **P2** has such orientations in opposite directions. The unit cell volume of the polymorph **P2** ($Z = 4$) has approximately twice the volume of the polymorph **P1** ($Z = 2$); it happend due to coalescence of two unit cells of **P1** in the *ab*-crystallographic plane. A mixed methanol/water solvate of the copper complex is also reported. It has a channel-like arrangement of the cations; has the anions and the solvents within the cation embraced channel-like enclosures. This complex is unstable, once taken out from the methanol solvent, it transforms in real time to **P2** by replacements of the methanol molecules by water molecules.
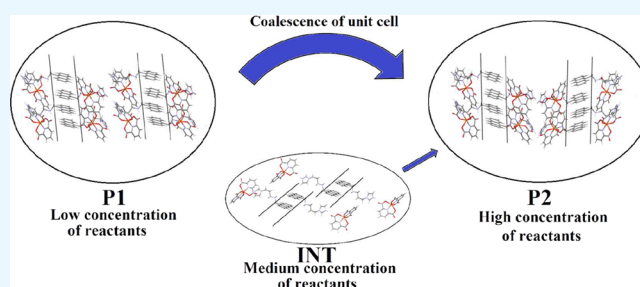
1. INTRODUCTION

The π-stacking among aromatic units have profound interest in fundamental,[1] biological,[2] and material sciences.[3] The magnitude of aromatic π-stacking interactions is very small (∼2 kJ mol⁻¹).[4] However, those contribute to design catalysts[5] and magnetic,[6] optical,[7] high energy materials.[8] Aromatic π-stacking in a self-assembly influences physical properties like conductance, proton transfer, etc.[9] Herringbone arrangement is a term used for organized π-stacks and has broad dimensions for material design.[10] The formations of Herringbone structures are guided by solvent,[11] host–guest interactions,[12] effect of substituents,[13] and stimuli.[14] Stacking among the phenyl rings occur in several ways such as edge-to-face, face-to-face, or oblique types, as illustrated in Figure 1a.[15] It may be seen that the face-to-face parallel molecules either having eclipsed (Figure 1a (iii)) or partly eclipsed (Figure 1a (vi)) geometries may be further arranged in different ways at translated positions in the case of eclipsed pairs, or as in a uni-directional manner (Figure 1a (vii)) or in bi-directions (Figure 1a (viii)). Further complicacies may be brought on them by arranging such layers as monolayers or bilayers or more and their combinations. Such self-assemblies may be extended infinitely or truncate as combination of different numbers of units. Two such possibilities by extending chains of parallel stacked anthracene rings in a unidirectional or bidirectional manner are shown in the Figure 1b (ix, x). Among the poly-aromatic compounds, various

structural and packing arrangements of anthracene-based compounds are well studied.[16] The stacking among anthracene rings largely influence the nature of self-assemblies[17] and are reflected in the self-assemblies of metal complexes with anthracene-based ligands.[18] The stacking arrangements of molecules differ from system to system and can result in different types of stacking arrangements, among which the Herringbone or lamellar structures have been known to provide independent properties originating from packing patterns.[19] The spatial organization of stacks among aromatic planes controlled by a flexible part shows an effect on photoluminescence.[20] We felt that a compound having unsymmetrical aromatic group such as the anthracenyl-group will be suitable to explore stacks among anthracenyl groups which may adopt lamellar or Herringbone arrangements, as shown in ix and x of the Figure 1b. There are three important requirements to observe such stacking patterns; (a) face-to-face stacks among the planar rings, (b) inclined stacks in the same direction with respect to a vertical axis, (c) there must be organized,
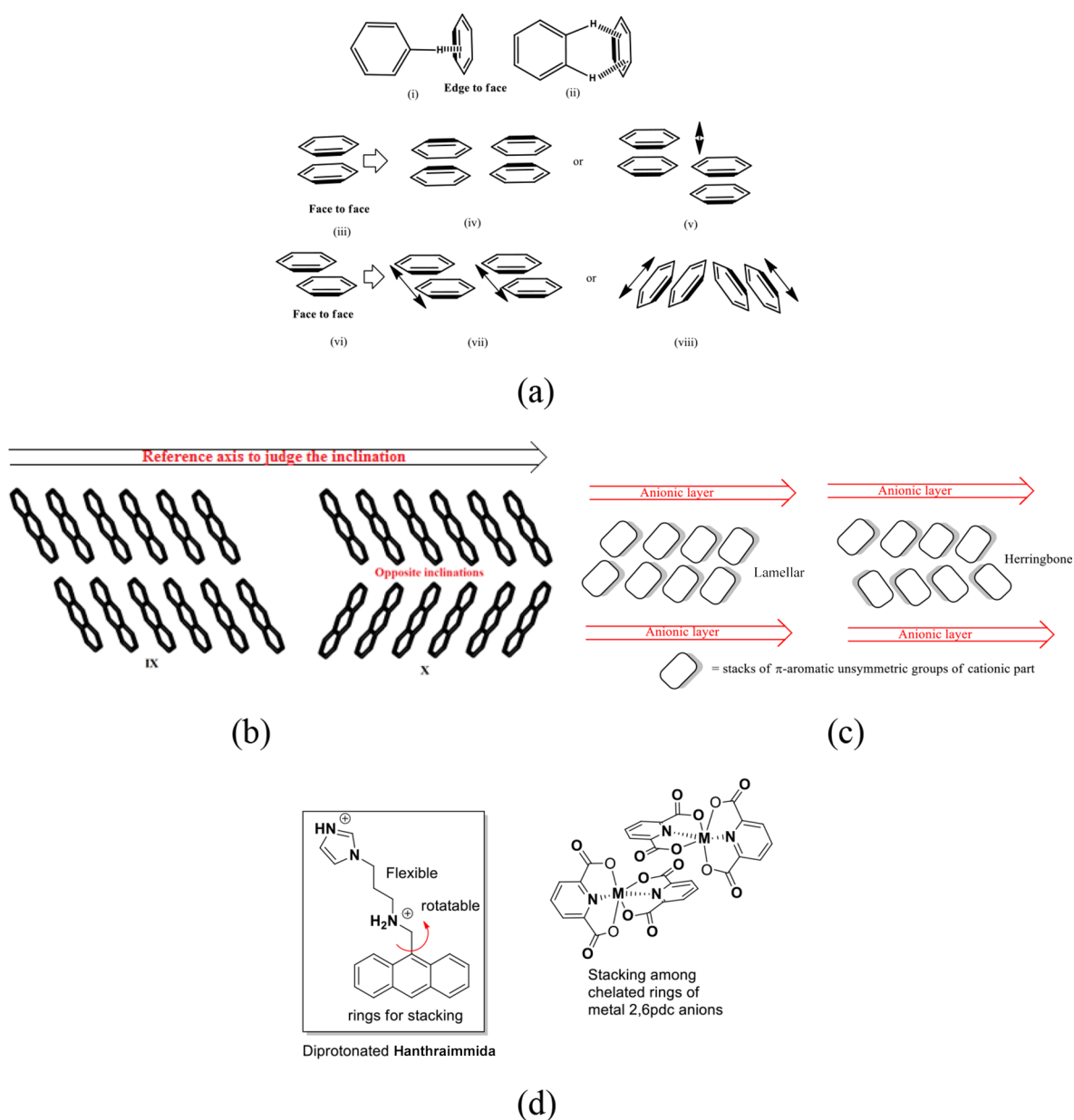
Figure 1. (a) Different π-interactions caused by the position and orientations of the stacked species shown by taking benzene as an example, (b) two different types of arrangements among the anthracene rings in parallel but in a (ix) unidirectional and a (x) bidirectional inclined manner. (c) Design principle for lamellar and Herringbone arrangements of the cationic part in a layered anionic reference frame. (d) Structure of dication from Hanthraimmida and the chelate-chelate stacks between 2,6-pyrdinedicarboxylate in its metal complex anion.

unidirection linear chains maintaining the slanting orientations to result lamellar structure or in the opposite directions to provide a Herringbone structure. These arrangements could lead to polymorphs but there has been no systematic approach available to obtain them, so we followed a design principle to organize stacks of π-components of a cationic part in layered anionic arrangements. For this purpose, we choose to study metal pyridine carboxylates having organic cation derived from 9-N-(3-imidazolylpropylamino)methyl anthracene (Hanthraimmida). The Hanthraimmida has a π-aromatic anthracenyl group appended though flexible linkers (Figure 1d). It is known to provide cocrystal with pyridine dicarboxylic acid,[21] where the organo cations of Hanthraimmida shows symmetry nonequivalent forms. The literature suggests that symmetry-independent molecules provide polymorphs[22] or synthon variations.[23] It is also known that the π-stacked 2,6-

pyridinedicarboxylate of a metal complexes having imidazolium cation form a layered structure.[24] Furthermore, the anionic part from metal-2,6-pyridinedicarboxylate complexes assemble as dimer (Figure 1d) involving the stacks of chelated ligands, and they are also known to form anionic 1-D-layer-like arrangements.[25] Hence, if the cationic part is derived from Hanthraimmida in such complexes, the anions will provide the required 1D arrangement to a set of anthracenyl group to form different stacking arrangements. The flexible tether to the anthracenyl unit would allow the anthracenyl unit to dictate the spatial orientations through interplay of weak interactions to provide polymorphs. With these backgrounds, we demonstrate here a pair of polymorphs that have lamellar and Herringbone arrangements of the anthracenyl groups and also an intermediate complex that provided the polymorph that has Herringbone arrangements.

Table 1. Crystallographic Parameters of the P1, P2, and INT

parameters	P1	P2	INT
formula	$Cu_2C_{70}H_{76}N_{10}O_{25}$	$Cu_2C_{70}H_{76}N_{10}O_{25}$	$CuC_{37}H_{41}N_5O_{12}$
CCDC	2250640	2250641	2250642
mol. wt.	1584.48	1584.48	811.29
crystal system	triclinic	monoclinic	triclinic
space group	$P\bar{1}$	$P2_1/c$	$P\bar{1}$
a (Å)	11.380(7)	11.338(4)	9.70(2)
b (Å)	15.195(10)	41.360(12)	13.71(3)
c (Å)	22.011(14)	15.328(5)	14.69(3)
α (°)	79.784(17)	90	78.23(4)
β (°)	75.809(17)	94.020(9)	79.74(5)
γ (°)	88.457(18)	90	83.84(7)
V (Å^3)	3631(4)	7170(4)	1877(7)
density, g cm^{-3}	1.449	1.468	1.435
abs. coeff., mm^{-1}	0.673	0.682	0.652
F (000)	1648	3296	846
total no. of reflections	12,769	12,633	6607
reflections, $I > 2\sigma(I)$	8107	8946	5464
max. $\theta/°$	24.999	25.000	25.000
ranges (h, k, l)	$-13 \leq h \leq 13$	$-13 \leq h \leq 13$	$-11 \leq h \leq 11$
	$-18 \leq k \leq 18$	$-49 \leq k \leq 49$	$-16 \leq k \leq 16$
	$-26 \leq l \leq 26$	$-18 \leq l \leq 18$	$-17 \leq l \leq 17$
complete to 2θ (%)	99.9	99.9	99.6
data/restraints/parameters	12,769/0/983	12,633/1/986	6607/0/500
GooF (F^2)	1.109	1.096	1.016
R indices [$I > 2\sigma(I)$]	0.0833	0.0523	0.0555
wR_2 [$I > 2\sigma(I)$]	0.1713	0.1125	0.1488
R indices (all data)	0.1391	0.0881	0.0704
wR_2 (all data)	0.2102	0.1395	0.1709

2. EXPERIMENTAL SECTION

9-N-(3-Imidazolylpropylamino) methyl anthracene was prepared by the reported procedure.[21]

2.1. Synthesis, Characterization, and Intermediate Isolation.
[(H$_3$anthraimmida)Cu(26pdc)$_2$]$_2$·9H$_2$O (**P1** and **P2**): To a well-stirred solution of 2,6-pyridinedicarboxylic acid (33.42 mg, 0.2 mmol) and copper(II) acetate monohydrate (19.96 mg, 0.1 mmol) in analytical grade methanol (20 mL), Hanthraimmida (31.54 mg, 0.1 mmol) was added. The resulting solution was stirred for about 1 h and kept undisturbed for crystallization in open conditions, which yielded flake-type crystals. The crystals were hand-picked after decanting the supernatant solution. (Isolated yield: 80%). Anal. calcd for C$_{70}$H$_{76}$Cu$_2$N$_{10}$O$_{25}$: C, 53.01%; H, 4.83%; N, 8.83%. Found: C, 52.70%; H, 5.60%; N, 8.87%. IR (cm^{-1}): 3375 (br, w, ν_{O-H}), 1614 (s, $\nu_{C=O}$), 1575 (s, $\nu_{C=N}$). Decomposition pt. 220.1 °C. UV−vis: 386 and 790 nm.

The same reaction was carried out with higher concentrations of the reactants used in the polymorph **P1** by keeping the volume of methanol the same (20 mL of methanol, and four times higher concentration of the reactants as that were used for preparation of **P1**) after stirring at room temperature for 12 h, provided a green precipitate. The precipitate formed was dissolved in water and the resulting solution was kept undisturbed for crystallization, under open air at 27 °C. After 5 days, the green crystals of **P2** appeared, and these were collected by decantation. (Isolated yield: 75%). Decomposition pt. 257 °C. Anal. calcd for C$_{70}$H$_{76}$Cu$_2$N$_{10}$O$_{25}$: C, 53.01%; H, 4.83%; N, 8.83%. Found: C, 52.80%; H, 4.95%; N, 8.87%. UV−vis: 370 nm and 806 nm. IR spectra of the **P2** was having insignificant difference from **P1**.

The intermediate [(H$_3$anthraimmida)Cu-(26pdc)$_2$].2.5H$_2$O.2CH$_3$OH (**INT**) was prepared by adding Hanthraimmida (63.08 mg, 0.2 mmol) to a well-stirred solution of 2,6-pyridinedicarboxylic acid (66.84 mg, 0.4 mmol) and copper(II) acetate monohydrate (39.92 mg, 0.2 mmol) in methanol (20 mL). The solution was stirred for about 3 h. On standing, bluish green crystals of **INT** appeared from the solution after 12 h; these crystals once taken out from solution were found to be unstable. The crystals were collected and put in paraffin oil and mounted in a diffractometer. The crystals of the complex once taken out from the solution became opaque and transformed to **P2**. This conversion was monitored under a microscope with time (please refer to the supplementary video). The IR of the neat crystals were immediately recorded by picking up the crystals from solution. The PXRD spectra of the fresh wet samples were recorded and had a matching pattern with the simulated one from the crystallographic information file (Figure 5S). IR (cm^{-1}): 3314 (br, w, ν_{O-H}), 2945 (s, ν_{C-H}) 1614 (w, $\nu_{C=O}$), 1575 (w, $\nu_{C=N}$), 1020 (s, ν_{C-O}).

2.2. Crystallographic Study.
The X-ray single crystal diffraction data for the salts were collected by a Bruker APEX-II CCD diffractometer at room temperature. Data refinement and cell reductions were carried out by Bruker SAINT Software. Data reduction and cell refinements were performed using SAINT and XPREP software. Structures were solved by direct methods using SHELXS-97 and were refined by full-matrix least-squares on F^2 using SHELXL-14 and OLEX2 programs. All non-hydrogen atoms were refined in anisotropic approximation against F^2 of all reflections. Hydrogen atoms were placed at their geometric positions by riding and refined in the isotropic approximation. The crystallographic parameters are listed in
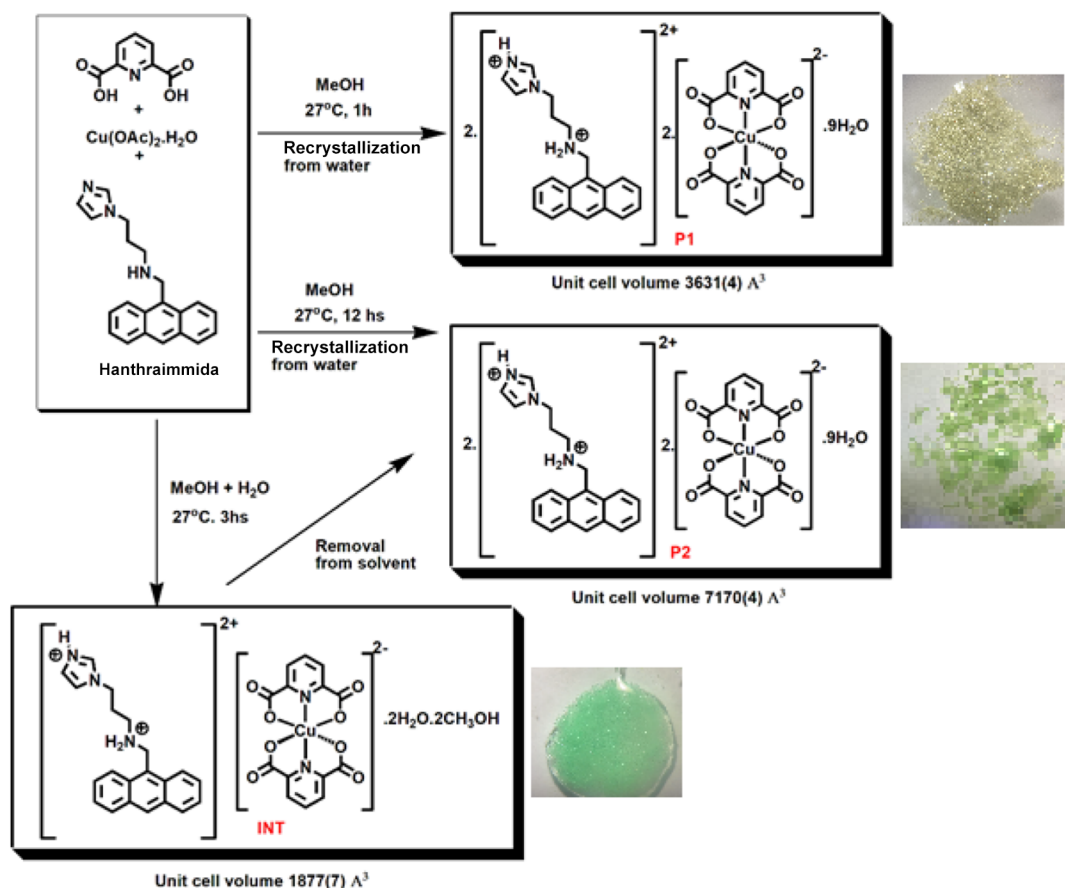
Scheme 1. Preparation of the P1, P2, and INT

Table 1.

For the structure of the **INT** solved at room temperature, a solvent mask was calculated by using OLEX2 software after removing all the solvent molecules. This showed that there were 119 electrons in a volume of 462 Å^3 in one void per unit cell. This is consistent with the presence of 2[CH$_3$OH], 2.5[H$_2$O] molecules per asymmetric unit to account the theoretical count 122 electrons per unit cell required for this composition. In case of the **INT** structure solved from data collected at low temperatures, a solvent mask was also calculated, and in this case, 116 electrons were found in a volume of 458 Å^3 in one void per unit cell. This is again consistent with the presence of 2[CH$_3$OH], 2.5[H$_2$O] per Asymmetric Unit to account for 122 electrons per unit cell within the constraints of experimental accuracy of X-ray diffraction. The formula presented in the Table 1 for **INT** reflects two water molecules as there was residual electron density accounting for half molecule of water. This residual density remained unresolved after several sets of data from independent data collection. The solvent percentage was confirmed by thermogravimetric analysis.

3. RESULTS AND DISCUSSION

Two different polymorphs of the complex [(H$_3$anthraimmida)-Cu(26pdc)$_2$]$_2$.9H$_2$O (26pdc = 2,6-pyridinedicarboxylate) were obtained at different time intervals from different concentrations of reactants from the reaction of 2,6-pyridinedicarboxylic acid with Hanthraimmida. A reaction performed at a relatively shorter duration (1 h) and at low concentration yielded the polymorph (**P1**). Whereas when the reaction with the same reactants continued for longer time (12 h) at relatively higher concentrations of the reactant, it resulted in the formation of another polymorph (**P2**). The same reaction at an intermittent concentration than the polymorphs but performed for approximately three hours provided another solvate of the complex, which was the intermediate [(H$_3$anthraimmida)Cu-(26pdc)$_2$]. The 2.5H$_2$O·2CH$_3$OH complex referred to as **INT** is shown in Scheme 1. The solid-state structures of all the complexes were characterized by single crystal X-ray diffraction. The intermediate complex **INT** was unstable, and once crystals of **INT** were taken out from the supernatant solution, it changed to the polymorph **P2**. Hence, it could not be isolated in bulk quantity and stored as the solid sample. We have taken out the complex and kept in an argon atmosphere for 30 min; under this condition also, the crystals were decomposed and the powder XRD of those crystal after 2 h resembled close to the polymorph **P2**. The crystal morphologies and color of the crystals of the solvate **INT** and the two polymorphs were different, those could be visually distinguished. The transformation of **INT** to **P2** could be also easily seen through the naked eyes, as the crystals of **INT** picked up from solution turns opaque and greenish yellow in real time. We have monitored the transformation by observing the crystals soaked in mother liquor placing them on a microscopic glass slide, placed under a microscope and recorded a video, which is enclosed as a Supporting Information (Video 1). The transformation in real time was clearly visible and suggested that the crystals comes closer once the solvent was getting evaporated from the glass plate and the crystal of the **INT** formed aggregated mass which provided the crystals of the **P2**. The crystals of **P1** and **P2** are stable and did not interconvert in the methanol solvent. The IR spectra (a and d Figure 2(i)) and
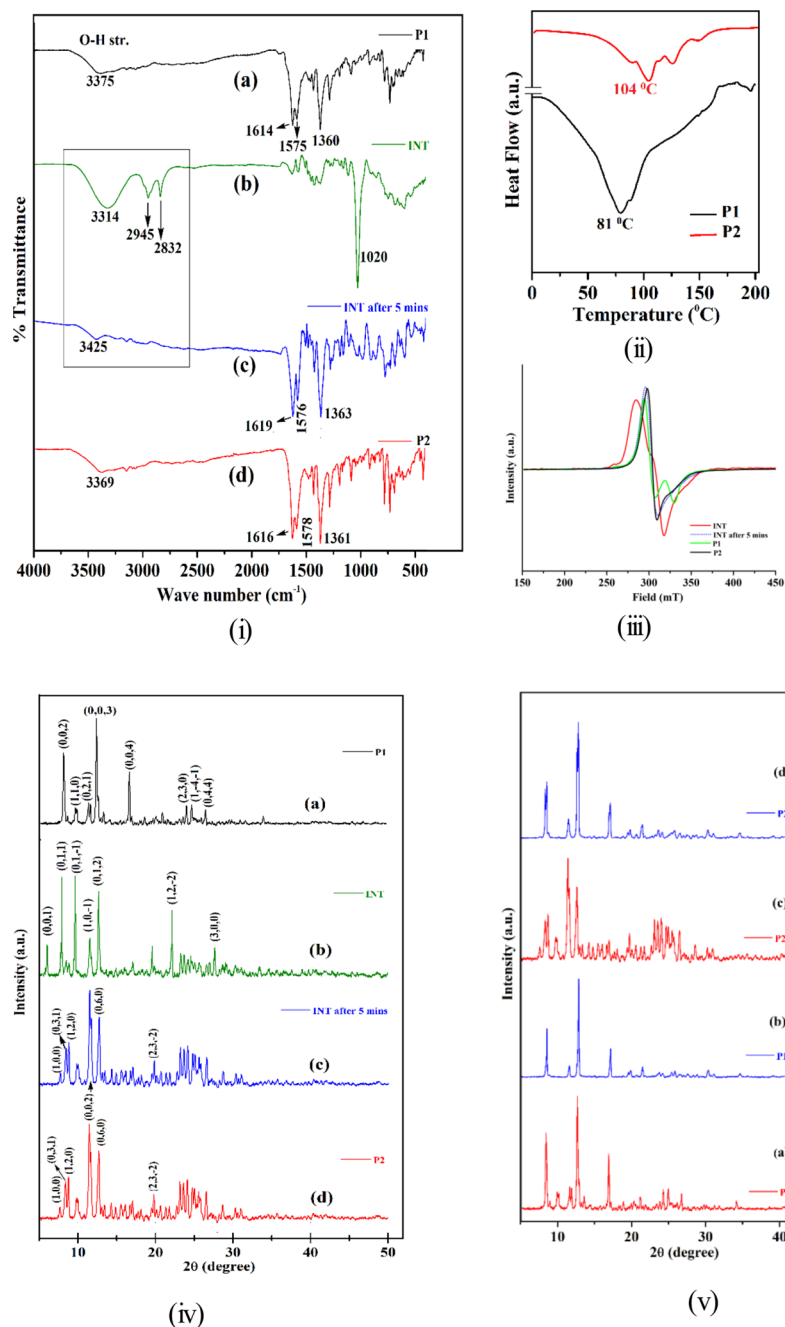
Figure 2. (i) IR (neat, cm^{-1}) spectra of the **P1** (a), **INT** immediately after preparation (b), **INT**, 5 min after taking out from the solution (c) and **P2** (d). (ii) DSC of the three forms heated up to 200 °C with a heating rate of 10 °C/min. (iii) Overlaid X-band ESR spectra of the solid samples of **P1**, **P2**, **INT**, and **INT** after 5 min at 297 K (calibrated with dpph $g = 2$). (iv) PXRD patterns of (a) **P1**, (b) **INT**, and (c) **INT** after 5 min and (d) **P2**. (v) PXRD patterns of (a) **P1**, (b) **P1** after heating at 150 °C, (c) **P2** and (d) **P2** after heating at 150 °C.

the elemental analysis of the **P1** and **P2** had close resemblances between them. Each polymorph had the characteristic IR peaks from the 26pdc at 1614–1619 cm^{-1}. The O−H stretches in each case was observed as a broad peak in the range of 3315–3375 cm^{-1}. The IR spectra of the solvate **INT** had differences from the polymorphs as it had showed a sharp peak at 3314 cm^{-1}. This IR-peak was used as to demarcate the instability of the **INT** crystals once taken out of the reaction medium. The crystals after 5 min loses the strong broad absorption at 3314 cm^{-1} (b of Figure 2(i)), and the IR spectra (c of Figure 2(i)), showed the peaks of the polymorph **P2**.

The thermal stability of two polymorphs were checked by recording their individual thermogram and differential scanning calorimetry (DSC) (Figures 9S−12S). From the TG, the polymorphs and the intermediate had showed weight loss due to the loss of the water of crystallization around, these were also reflected in the corresponding DSCs (Figure 2(ii)) around 81 °C (heating rate 10 °C), whereas, the polymorph **P2** had lost the water molecules at 104 °C. The polymorph **P1** was decomposed above 242 °C, and the **P2** was decomposed above 264 °C. In order to check the transformation between the two forms, we have recorded the DSC up to 120 °C (heating rate 5 °C) (Supporting Figures 13S and 14S). As the polymorphs were
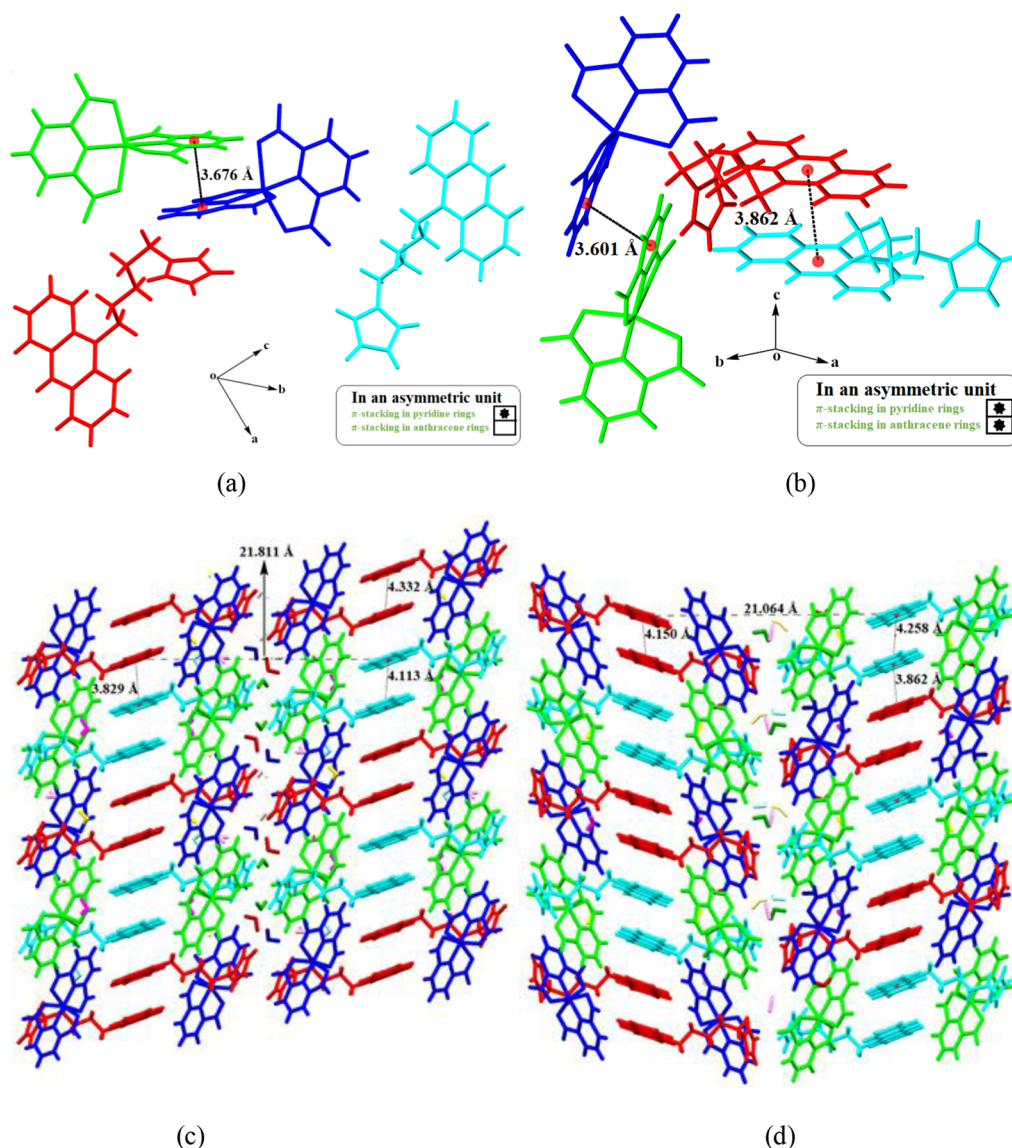
(a)   (b)

(c)   (d)

Figure 3. Crystal structure of (a) **P1** and (b) **P2** (water molecules are omitted for clarity) and the packing patterns of (c) **P1** and (d) **P2** showing the orientations of π-stacks in the two polymorphs.

decomposed above 242 °C, DSC plots of the polymorphs up from 0° to 120 °C were recorded, followed by cooling in a cyclic manner. The **P1** showed a broad endothermic peak at 54−93 °C, whereas the **P2** had showed multiple endothermic peaks in the range 60°−111 °C due to loss of water molecules (Supporting Figures 14S and 15S). Both the polymorphs in their respective cooling cycle did not show the original peak observed in the first cycle in this temperature range, showing no absorption of water by the dehydrated sample took place. The DSC curve of **INT** is also enclosed (Figure 17S), and it is quite similar to that of **P2**, as it was reported earlier in the text that **INT** is unstable after removal from the solvent. The thermogram of **INT** indicates a weight loss of approximately 13.29%, indicating the removal of solvent molecules consisting of two methanol and two and half water molecules. To ensure the stability of molecule during the collection of data, the TG measurement was conducted at a rate of 50 °C/min as **INT** is unstable at room temperature for a longer period of time. The DTG curve reveals a peak at 65 °C, indicating the loss of methanol molecules and another peak at 138 °C, indicating the

loss of water. The IR spectra of the fresh sample of **INT** has the methanol C−H stretches at 2945 and 2832 cm^{-1} which disappeared upon standing and shows a broad peak at 3425 cm^{-1} (ν_{OH}) due to replacement of methanol by water.

The X-ray photoelectron spectra of both the polymorphs were not distinguishable, but they confirmed the presence of copper(II) ions (Figures 6S and 7S). The ESR spectra of the **P1** had characteristic peaks of perpendicular and parallel components of g_{av} = 2.18 of copper(II) in a distorted octahedral geometry (Figure 2(iii)). The **P2** had showed a broad peak for the perpendicular component of g_{av} = 2.21 and the parallel component was not distinct, and the **INT** showed peak at g_{av} = 2.19. The ESR peak of the **INT** Figure 2(iii) observed in the fresh sample immediately transformed to show the peak of the polymorph **P2**. Experimentally determined powder XRD patterns of the **P1**, **P2**, and **INT** are shown in (Figure 2(iv)a,b, and d). The pattern of each form of the complex was compared with the respective powder XRD generated from their crystallographic information file (CIF) by using Mercury software (Supporting Figures 3S−5S). Each experimentally
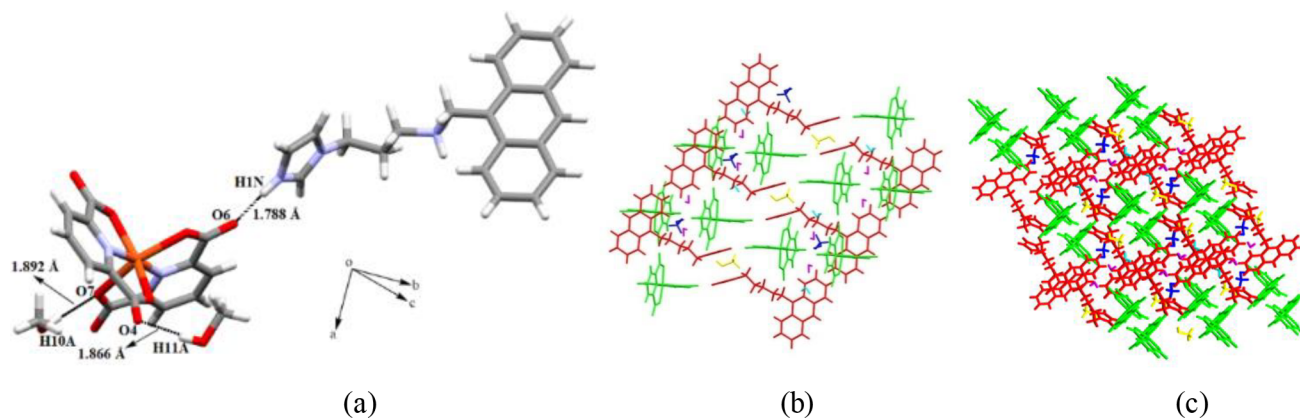
Figure 4. (a) Crystal structure of **INT**, showing hydrogen bonds of the anion with methanol molecules and cations, (the water molecules are omitted for clarity), (b) enclosures created by the π-embracing among the cations providing the surrounding to accommodate that solvent and anions. (c) The channels including the water and methanol molecules.

determined PXRD matched well with the respective one generated from CIF, showing the phase purity of the bulk samples. The transformation of **INT** to **P2** was reflected in the instantaneously recorded PXRD of the freshly prepared **INT** (c of Figure 2(iv)), it had a matching peak with the PXRD generated from its CIF, showing only one form in the crystals. Once the PXRD of the same sample was re-recorded, it was found that the PXRD was matching with the PXRD of the **P2** (d of Figure 2(iv)). The textures of the crystals were also changed. This occurred due to the replacements of the methanol molecules from the crystals by incorporation of water molecules. The **P1** and **P2** were independently desolvated each by heating at 150 °C for 2 h in an oven. The PXRD patterns of both the samples were recorded and both transformed to a common form. It was found that the anhydrous form of the **P1** had a similar pattern as that of the hydrate. The X-ray diffraction pattern of the dehydrated form of **P2** was similar to the dehydrated form of **P1** (Figure 2(v)).

3.1. Crystal Structures. We have determined the X-ray crystal structure of both the polymorphs and also of the intermediate complex **INT**. For the structure determination of **INT**, the crystals were placed in paraffin oil and a good diffracting crystal was picked up to collect the diffraction data immediately. The crystal structures of the two polymorphs **P1** and **P2** had showed that both had two symmetry independent molecules; that is to suggest that they had two symmetry independent cations as well as two anions in their respective asymmetric unit; this was apart from each having nine water molecules. In fact, these should be considered to have 4.5 moles of water per complex from chemical point of view. Each organic cation in the structures of the **P1** and **P2** had independent orientations of the imidazole unit with respect to the anthracenyl group; and conformation of those organocations were not equivalent. The structure of the two polymorphs are shown in the Figure 3a,b. The coordination environment around copper(II) ion, of the both polymorphs were identical having two 2,6-pyridinedicarboxylates coordinated to copper(II) ion each providing NO_2 type of coordination environment. The metal−ligand bond parameters are listed in supporting Table 3S. In the unit cell of each polymorph, there were two symmetry independent hexa-coordinate $[Cu(26pdc)_2]^{2-}$ anions; and the two chelated unit of the complex were found as stacked dimers. This is not unusual as there are large numbers of chelate complexes where stacking among the coordinated ligands form

assemblies[26] and 2,6-pyridinedicarboxylate complexes[24,25] are not exception to those. The distance between the two planes of stack dimers of the anions, in **P1** was 3.676 Å, and in **P2**, it was 3.601 Å. There were also two symmetry independent dications in the respective unit cell of each polymorph. These organic dications were formed by protonation of Hanthraimmida at the N−H next to anthracenyl group and at the sp^2-N atom of the imidazole. The imidazolium portion of the cations were involved in the formation of charge-assisted hydrogen bonds. Both the $^+$N−H$_{(imidazole)}$ of the symmetry-independent cations of **P1** were hydrogen-bonded to the anions through intervening water molecules. It had two types of $^+$N−H$_{(imidazole)}$···O$_{(water)}$ hydrogen bonds connecting the anions. In one site, there were two intervening hydrogen-bonded water molecules, and in another site, there was one intervening hydrogen-bonded water molecule. In **P2**, the two imidazolium cations were involved in hydrogen bonds in a different manner, and it had $^+$N−H$_{(imidazole)}$···O$_{(water)}$ and $^+$N−H$_{(imidazole)}$···O$_{(26pdc)}$ hydrogen bonds contributing to the assembly. Both the polymorphs had independent types of chain-like arrangements among the cations and anions; these chains were organized in such a way that anthracene rings from two independent chains. These chains were assembled in face-to-face stackings to form layer-like arrangements. The rings were inclined with respect to the anionic chains. Those bilayers of the **P1** were oriented in the same direction, providing a lamellar structure, whereas, in the case of **P2**, the layers were organized in the opposite directions as alternate bilayers to provide the herringbone structure. These arrangements provided differences in the packing of the two polymorphs. In the literature, flexible dyads such as of monoalkoxynaphthalene−naphthalimide undergoes thermochromic transformation due to changes in the π-stacks.[23] In such systems, the flexible alkyl chains had a role to guide the stacks. In the present example, we had $(CH_2)_3$-tether linking the anthracenyl group with the imidazolium cation. Thus, there were various conformations to guide the orientations of those rings and to bring in varieties in the self-assemblies. It may be noted that the bisphosphoramidate and its methanol solvate were reported to have single and two molecules in the asymmetric units; in that case, the packing patterns were guided by edge to face C−H···π interactions.[27] Our examples had two symmetry independent molecules with lamellar and Herringbone arrangements that have provided avenues for a new polymorphic compounds of such a kind.

In the crystal structure of the **INT**, the asymmetric unit had a $[Cu(26pdc)_2]^{2-}$ anion and a H_3anthraimmida cation (Figure 4a). One of the carbonyl oxygen atom of the $[Cu(26pdc)_2]^{2-}$ was hydrogen bonded to the N-H of imidazolium unit on the cation. This compound had also anthracene rings in parallel positions, but those were located at translated positions. The packing diagram of **INT** showing the encapsulated anions in cationic enclosures is shown in Figure 4b,c. There were non-eclipsing parallel rings of the anthracenyl group as pairs along the *b*-crystallographic direction. The planes of these anthacenyl-groups had a centroid to centroid distance of 4.56 Å. This distance suggested no stacking interactions among the anthracenyl groups. In the self-assembly, four neighboring cations were organized by forming hydrogen bonds through the oxygen atoms of C=O of the anions with the N−H bond of the $-^+NH_2-$ unit of the cation. They provided laterally embraced enclosures of anthracenyl groups to encapsulate two $[Cu-(26pdc)_2]^{2-}$ anions (Figure 4b). A view along the *b*-crystallographic axis showed these enclosures as channel-like arrangements. The anions were encapsulated in these cation embraced channel-like structure.

The water molecules in the self-assembly contributed to segregate the anions by providing hydrogen-bonded bridges connecting anions in another channel. In the overall assembly, a view from the *bc*-plane showed that the anions were in pairs formed through the stacks between the two chelated ligands. Those stacked ligands of the $[Cu(26pdc)_2]^{2-}$ were separated by a centroid to centroid distance 3.55 Å; on the other hand, the anions within the channels were held apart without stacks among them. Therefore, there was possibly a tendency to break the barricades of the channels to form the stacked arrangements among the anions. This could be a factor for the **INT** transforming to the **P2**. The **INT** is an anion encapsulated assembly in a cationic noncovalent enclosure, and there are examples of such class reported in the literature based on different methodologies.[28] The channel-like arrangements of noncovalent structures are useful to assemble and disassemble to facilitate ion transport.[26] In our case, we found that this structure was very unstable and turned to π-stacked structure spontaneously upon exposure to moisture or removal of the solvent. The structure of **P2** had Herringbone cross-beddings structures, which relates to the structures of sediments formed on the sea shores by tides. Those structural patterns have a look of the structural arrangements of the bones of a fish. Such patterns on the soil in a sea-shore occurs due to periodic flows of water during the forward and backward movement of water in tide and ebb. Those periodic patterns have the fore-sets in successive parallel structured arrangements in opposite directions.[29] There are also examples of self-assemblies where changes in the stacking among the molecules caused gate opening and enabled to design in the artificial ion channel by externally adding a π-stacking component.[30] In the present case, there was spontaneous formation of polymorph **P2** having a Herringbone cross-bed structure, from the intermediate complex **INT**. The transformation resulted in **P2** which had extensive stacking among the rings. The channel-like arrangements of **INT** broke down upon replacement of methanol molecules by water. In this case, the molecules of solvents once get apart, the molecule reorganizes to form the one form that has stacking among the planar portions of the anions as well as among the cations. Accordingly, the solvent molecules get into the respective positions of the stable form of the polymorph. This process is favorable as methanol is a low boiling solvent, and it escapes

easily from the lattice to get replaced by water that has a higher hydrogen bonding ability. Attempted synthesis of only methanol solvate of the complex in dry methanol in inert atmosphere yielded **INT**, suggesting the propensity of it to crystallize out as solvate having methanol and water together. The **INT** had two and half water molecules and two methanol molecules.

The polymorph **P2** had 4.5 water molecules per complex; although crystallographically, there were 9 molecules per unit cell that has two complex molecules in the unit cell holding those. Theoretically, at ambient conditions, the volume of a molecule of methanol is 6.9×10^{-23} cm^3 and the volume of a water molecule is 2.98×10^{-23} cm^3. There were 4.5 molecules of water of the polymorph **P2** (per complex) that has a volume of 12.06×10^{-23}. However, **INT** has two and half water molecules together with two methanol molecules and has a volume 21.25×10^{-23} cm^3. As replacement of methanol by water will require lesser volume, hence replacement of methanol by water was possible. Furthermore, the water molecules have much higher numbers of hydrogen bond sites than that of methanol to provide a stable structure. Accordingly, the incorporation of water molecule to expel out the methanol molecules of the **INT** was feasible with a minimal volume changes. There are known 1,10-phenanthroline solvates having different π-stacks and certain ones are transient; after removal from the mother liquor, it also forms a hydrate with Z′ = 3.[31a] The role of the solvent in such a case is to provide pivot to guide the orientations of the ring; in an earlier study, we also had shown the role of DMSO and DMF to provide different sets of hydrogen bonding environment resulting in Z′ = 1 or 2.[31b] In the present case, there were stacked dimers of anions that provided the pivot in each case to link to the organic cations, by direct hydrogen bonds or through intervening water molecules. The orientations of the anion dimers were different, and the assembling of these guided the orientations of the cations to have different Z′. It was shown that the hydrates having a lower amount of water molecules provide channel-like structures[31] and we do find a similar aspect having channel-like structure in the **INT**. The structure of the **INT** at low temperatures (120 K, the CCDC No. 2265340) was determined; in this case, it had 2.5 water molecules and two methanol molecules in the complex as the solvent of crystallization. We could not resolve the crystallographic disorder in the water molecules in the structure. Hence, the structure was solved by squeezing the water molecules and the CIF of the structure is enclosed as Supporting Information. There was least change in the unit cell parameters with respect to the unit cell parameters at room temperature, confirming it to be the same structure. These discussions as well as the observations relating to the channel, suggest its propensity to form stacked structures through easy loss of the methanol molecules from the channels. The transformation took place by accepting water molecules from the solvent (99% methanol) to replace methanol; water is a better hydrogen bond forming species than methanol and to utilize higher numbers of hydrogen bonds than methanol to provide stability.

3.2. Structural Comparison Relating Conversion of Polymorphs and Solvate.

We had sorted out the dihedral angles that contributed to the orientations to the planar anthracenyl rings by focussing on the flexible portion of the single bonded $-(CH_2)_3-$ tether. The dihedral angles were found to be different for the symmetry independent cations in both the polymorphs (listed in Table 4S). A better picture was obtained by drawing the overlaid diagram of the cations by keeping the anthracenyl group of each cation fixed as eclipsing
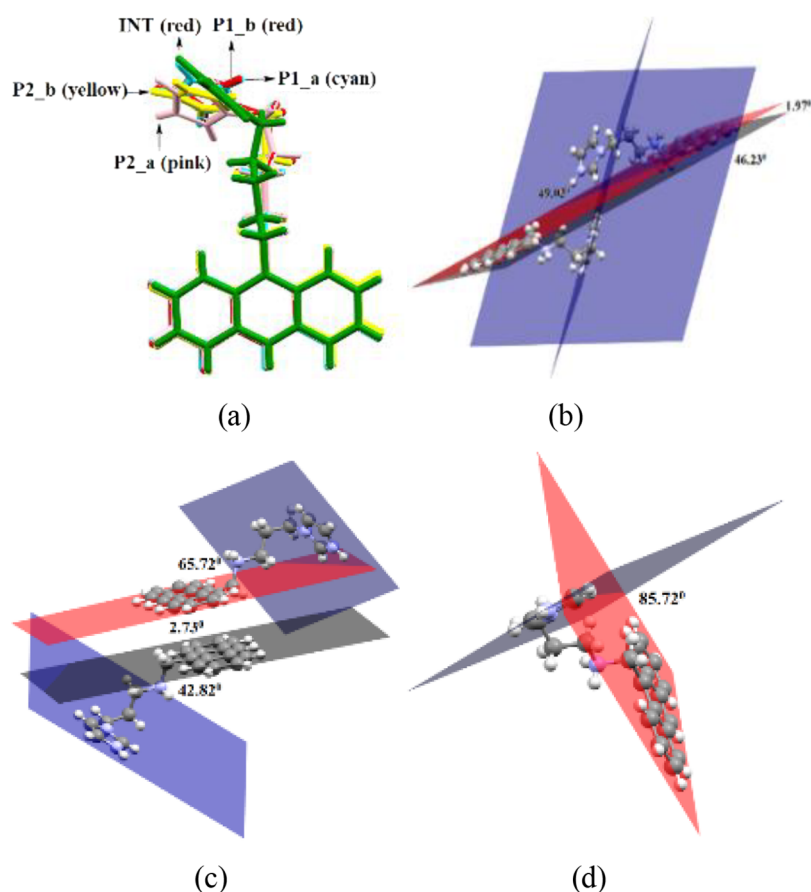
Figure 5. (a) Overlaid diagram of the cations of the **P1**, **P2**, and **INT** showing the differences in the orientations of the imidazolium cation with respect to anthracene ring (_a and _b represent symmetry independent cations of the unit cell of the respective polymorph). The angles between independent planes constructed over the rings of the anthracene and imidazolium part of each cation of (b) **P1**, (c) **P2**, and (d) **INT**.

each other with respect to the plane of the paper (Figure 5a). In **P1** and **P2**, the symmetry-independent cations had differences in the angular orientations shown by designating them by _a and _b in Figure 5a. The spatial dispositions of the $^+$N−H$_{(imidazole)}$ in **P1** were toward same side, whereas in **P2**, these were projected inward and outward toward the anthracenyl group. The most intriguing feature is that the projection of the $^+$N−H$_{(imidazole)}$ in the two polymorphs are in opposite direction in such an overlaid diagram. This is one of the key issue the hydrogen bond as the $^+$N−H$_{(imidazole)}$ participated in both the polymorphs and contributed to provide the directionality to the respective self-assembly. In the case of the **INT**, the cation had orientation of the $^+$N−H$_{(imidazole)}$ resembling of one of the cation marked red in Figure 4a. To be more precise, these affected the orientations of the planes drawn including the planar anthracenyl group of individual cation with respect to the plane drawn on the plane of the imidazole ring. The angles bisecting those two planes of the cations of the **P1** were 43.03° and 46.23°, respectively (Figure 4c−e), whereas those were 65.72° and 42.82° in **P2**. The cation of **INT** had the bisecting angle 85.72°. Hence, the similar orientations of the $^+$N−H$_{(imidazole)}$ of the one cation of **P2** with the cation of the **INT** was not guiding the bisecting angle between the two planes and it was the central tether that made the difference in this orientations of the planes. This analysis had clarified that the only one bisecting angle between the anthracenyl part; and the imidazole part of **P2** had a significant difference from the other three orientations that had close similarities of the bisecting angles. This provided different

inclinations among the rings as proposed to have provided the Herringbone arrangement in **P2**.

The crystals of the **P1** belonged to the triclinic P-1 space group, whereas the crystals of the **P2** belonged to monoclinic $P2_1/c$. There were large differences in the unit cell volumes of the two polymorphs, **P1** has a volume 3631(4) Å^3, whereas the **P2** has a volume about twice of this, precisely 7170(4) Å^3. There was a large difference in the length of the b-crystallographic axis, for **P1**, it was 15.195(10) Å, whereas for **P2**, it was 41.360(12) Å. Crystal densities of the polymorphs were similar. The intermediate complex **INT** was crystallized in the triclinic $P −$ 1 space group. It has a unit cell volume 1877(7) Å^3 which is about four times smaller than the respective volume in **P2** ($z =$ 4), but about half the volume of the **P1** ($z = 2$). On the other hand, the two symmetry-independent molecules in the unit cell of each polymorph were with different torsion angles (Table 4S). Hence, the systems are complicated to understand in a straight forward manner, it requires answers to accommodate the consequences of solvents to to guide the arrangements to have the symmetry independent molecules. This aspect is a push forward to have new insight into the varieties in conformational flexible molecules in solid-state self-assemblies. In this regard, we had an advantage that both **P1** and **P2** had the same numbers of symmetry independent molecules and there was a doubling in unit cell. The analysis on the unit cell suggested that if two unit cells of **P1** along ab-crystallographic faces were overlapped, it would provide similar packing to the **P2**. Hence, it was possible to generate the coalesced unit cell, that was very similar to the
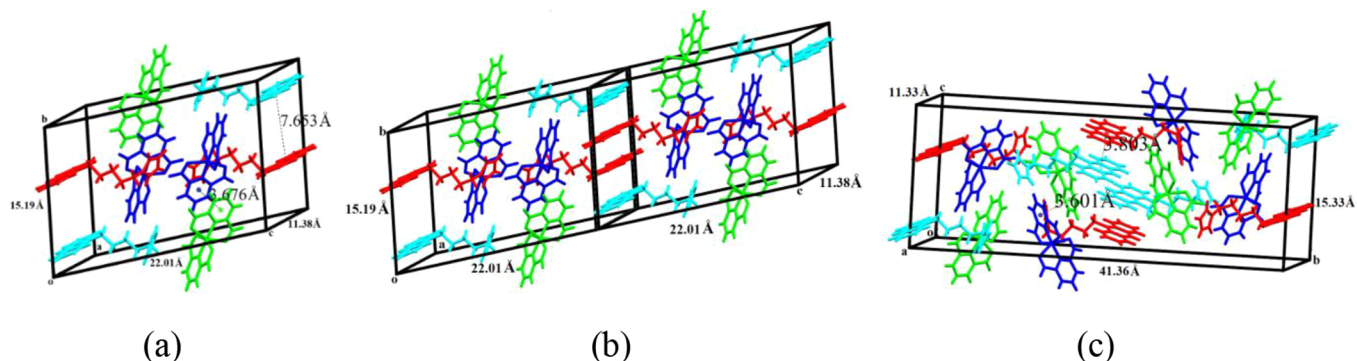
Figure 6. Different unit cells to show the doubling of unit cell volume through π-stacking, (a) Unit cell of **P1**, (b) coalescence of *ab*-crystallographic faces of two unit cells of **P1**, and (c) unit cell of **P2**.

unit cell of **P2** (Figure 6). This coalescence had accommodated the required π-stacking among the anthracenyl groups that was present in the **P2** (Figure 6b). The doubling of unit cell volumes occurs in inorganic compounds due to electronic effect[32a] and deformation of geometry.[32b] Doubling and quadruplet increase in volumes of unit cell among polymorphs without conformational changes of the molecules were reported earlier.[32c] We also had reported the extended domain as a factor to enhance unit cell volumes in polymorphic solvates.[32d] The evaporation rates of solvents also provide time-dependent π-stacks among donors and acceptor molecules.[33] and our results showed this aspect as a new example. In this study, the additional point is on the role of concentration dependence together with time dependence in the formation of the three forms of the complex. Indeed, we observe a similar propensity to form stacks among the planar units. Switching between π-systems from one form to other;[34] their property changes[35] and desolvation leading to isostructural forms[36] are well known. The hydrolysis of ester containing complex in the solid state converting to crystalline carboxylate compound was reported by us.[37] In the present case, the formation of the **P2** from the **INT** involved very small amount of mass loss, but it caused while getting converted to **P2** about 4-times increase in the unit cell volume from **INT** had occurred, and it was not a single crystal to single crystal transformation.

4. CONCLUSIONS

Two polymorphs having lamellar or Herringbone arrangements of the anthracenyl groups were formed under different crystallization conditions due to the propensity to maximize π-stacks among planar anthracene rings. In these examples, the copper-pdc anions served as hinges to the cations in different ways to influence the spatial orientations of the anthracenyl groups deciding the extent of face-to-face π-stacking among them. The most important aspect observed in this study was the **P2** ($z = 4$) having double the unit cell volume that of **P1** ($z = 2$) that occurred due to assembling of two unit cells along *ab* crystallographic faces through π-stacking. The coalescence of two independent unit cells of a polymorph through π-stacking converting to another polymorph is unprecedented and open a new avenue for understanding. This study also have illustrated the fact that assemblies in solution at different concentration could provide crystallization of mixed solvate as intermediate **INT**, which transformed to **P2** by the replacement of methanol from channel-like enclosures of the **INT** to maximize hydrogen bonds and π-stacking.

■ ASSOCIATED CONTENT

Data Availability Statement

The crystallographic information files are submitted to the Cambridge Crystallographic Database center and have the CCDC numbers 2250640−2250642, 2265340.

ⓈI Supporting Information

The Supporting Information is available free of charge at https://pubs.acs.org/doi/10.1021/acsomega.3c05132.

> PXRD patterns; UV−visible spectra; TG and DSC; PES; hydrogen bond tables; and selected torsion angles of the polymorphs; general aspects of experimental section, crystallographic parameters; and hydrogen bonds (PDF)
> Video on the crystal of **INT** transforming to **P2** is also included (MP4)

■ AUTHOR INFORMATION

Corresponding Author

Jubaraj B. Baruah − *Department of Chemistry, Indian Institute of Technology Guwahati, Guwahati 781 039 Assam, India;* ⓞ orcid.org/0000-0003-3371-7529; Phone: +91-361-2582311; Email: juba@iitg.ac.in; Fax: +91-361-2690762

Author

Abhay Pratap Singh − *Department of Chemistry, Indian Institute of Technology Guwahati, Guwahati 781 039 Assam, India*

Complete contact information is available at:
https://pubs.acs.org/10.1021/acsomega.3c05132

Author Contributions

The manuscript was written through contributions of both authors. Both authors have given approval to the final version of the manuscript.

Notes

The authors declare no competing financial interest.

Physics, IIT Guwahati, for help in recording the video of the crystal transformation.

■ REFERENCES

(1) (a) Martinez, C. R.; Iverson, B. L. Rethinking the term "pi-stacking". *Chem. Sci.* **2012**, *3*, 2191−2201. (b) Janiak, C. A critical account on π−π stacking in metal complexes with aromatic nitrogen-containing ligands. *J. Chem. Soc., Dalton Trans.* **2000**, 3885−3896. (c) Jennings, W. B.; Farrell, B. M.; Malone, J. F. Attractive intramolecular edge-to-face aromatic interactions in flexible organic molecules. *Acc. Chem. Res.* **2001**, *34*, 885−894. (d) Bora, P.; Saikia, B.; Sarma, B. Regulation of π···π stacking interactions in small molecule cocrystals and/or salts for physiochemical property modulation. *Cryst. Growth Des.* **2018**, *18*, 1448−1458. (e) Deng, J. H.; Juo, J.; Mao, Y. L.; Lai, S.; Gong, Y. -N.; Zhong, C.; Lu, T. B. π-π stacking interactions: Non-negligible forces for stabilizing porous supramolecular frameworks. *Sci. Adv.* **2020**, *6*, EAAX9976. (f) Wheeler, S. E.; Bloom, J. W. G. Toward a more complete understanding of noncovalent interactions involving aromatic rings. *J. Phys. Chem. A* **2014**, *118*, 6133−6147. (g) Thakuria, R.; Nath, N. K.; Saha, B. K. The nature and applications of π−π interactions: A perspective. *Cryst. Growth Des.* **2019**, *19*, 523−528. (h) Guijarro, A.; Verges, J. A.; San-Fabian, E.; Chiappe, G.; Louis, E. Herringbone pattern and CH-π bonding in the crystal architecture of linear polycyclic aromatic hydrocarbons. *ChemPhysChem* **2016**, *17*, 3548−3557.

(2) (a) McGaughey, G. B.; Gagne, M.; Rappe, A. K. π-Stacking interactions, alive and well in proteins. *J. Biol. Chem.* **1998**, *273*, 15458−15463. (b) Kool, E. T. Hydrogen bonding, base stacking, and steric effects in DNA replication. *Annu. Rev. Biophys. Biomol. Struct.* **2001**, *30*, 1−22. (c) Chen, T.; Li, M.; Liu, J. π−π stacking interaction: A nondestructive and facile means in material engineering for bio-applications. *Cryst. Growth Des.* **2018**, *18*, 2765−2783. (d) Cooper, V. R.; Thonhauser, T.; Puzder, A.; Schroder, E.; Lundqvist, B. I.; Langreth, D. C. Stacking interactions and the twist of DNA. *J. Am. Chem. Soc.* **2008**, *130*, 1304−1308. (e) Iwaura, R.; Yui, H.; Someya, Y.; Kameyama, M. O. Construction of energy transfer pathways self-assembled from DNA-templated stacks of anthracene. *J. Photochem. Photobiol. B* **2014**, *130*, 199−204. (f) Meyer, E. A.; Castellano, R. K.; Diederich, F. Interactions with aromatic rings in chemical and biological recognition. *Angew. Chem., Int. Ed.* **2003**, *42*, 1210−1250. (g) Dhar, J.; Karothu, D. P.; Patil, S. Herringbone to cofacial solid state packing via H-bonding in diketopyrrolopyrrole (DPP) based molecular crystals: influence on charge transport. *Chem. Commun.* **2015**, *51*, 97−100.

(3) (a) Curtis, M. D.; Cao, J.; Kamp, J. W. Solid-state packing of conjugated oligomers: From π-stacks to the herringbone structure. *J. Am. Chem. Soc.* **2004**, *126*, 4318−4328. (b) Sutton, C.; Risko, C.; Brédas, J. -L. Noncovalent intermolecular interactions in organic electronic materials: implications for the molecular packing vs electronic properties of acenes. *Chem. Mater.* **2016**, *28*, 3−16. (c) Egbe, D. A. M.; Turk, S.; Rathgeber, S.; Kuhnlenz, F.; Jadhav, R.; Wild, A.; Birckner, E.; Adam, G.; Pivrikas, A.; Cimrova, V.; Knor, G.; Sariciftci, N. S.; Hoppe, H. Anthracene based conjugated polymers: Correlation between π−π-stacking ability, photophysical properties, charge carrier mobility, and photovoltaic performance. *Macromolecules* **2010**, *43*, 1261−1269. (d) Gierschner, J.; Shi, J.; Milian-Medina, B.; Roca-Sanjuan, D.; Varghese, S.; Park, S. Y. Luminescence in crystalline organic materials: from molecules to molecular solids. *Adv. Opt. Mater.* **2021**, *9*, No. 2002251. (e) Hashizume, D.; Nakano, M.; Ogaki, T.; Takenaka, H.; Kawabata, K.; Takimiya, K.; Wang, C. "Disrupt and induce" intermolecular interactions to rationally design organic semiconductor crystals: from herringbone to rubrene-like pitched π-stacking. *Chem. Sci.* **2020**, *11*, 1573−1580. (f) Bhat, V.; Gopan, G.; Nair, N. G.; Hariharan, M. γ-Herringbone polymorph of 6,13-bis(trimethylsilylethynyl)pentacene: A potential material for enhanced hole mobility. *Chem. − Eur. J.* **2018**, *24*, 8679−8685.

(4) Jorgensen, W. L.; Severance, D. L. Aromatic-aromatic interactions: Free energy profiles for the benzene dimer in water, chloroform, and liquid benzene. *J. Am. Chem. Soc.* **1990**, *112*, 4768−4774.

(5) Neel, A. J.; Hilton, M. J.; Sigman, M. S.; Toste, F. D. Exploiting non-covalent π interactions for catalyst design. *Nature* **2017**, *543*, 637−646.

(6) (a) Reger, D. L.; Debreczeni, A.; Reinecke, B.; Rassolov, V.; Smith, M. D.; Semeniuc, R. F. Highly organized structures and unusual magnetic properties of paddlewheel copper(II) carboxylate dimers containing the π−π stacking, 1,8-naphthalimide synthon. *Inorg. Chem.* **2009**, *48*, 8911−8924. (b) Tsuji, Y.; Okazawa, K.; Kurino, K.; Yoshizawa, K. Topology dictates magnetic and conductive properties of a π-stacked system: insight into possible coexistence of magnetic and conductive systems. *J. Phys. Chem. C* **2022**, *126*, 3244−3256. (c) Huang, J.; Kertesz, M. Intermolecular covalent π-π bonding interaction indicated by bond distances, energy bands, and magnetism in biphenalenyl biradicaloid molecular crystal. *J. Am. Chem. Soc.* **2007**, *129*, 1634−1643.

(7) Jin, M. Y.; Zhen, Q.; Xiao, D.; Tao, G.; Xing, X.; Yu, P.; Xu, C. Engineered non-covalent π interactions as key elements for chiral recognition. *Nat. Commun.* **2022**, *13*, 3276.

(8) (a) Li, S.; Gou, R.; Zhang, C. π−π Stacking in energetic crystals. *Cryst. Growth Des.* **2022**, *22*, 1991−2000. (b) Zhang, C.; Wang, X.; Huang, H. π-stacked interactions in explosive crystals: Buffers against external mechanical stimuli. *J. Am. Chem. Soc.* **2008**, *130*, 8359−8365. (c) Bu, R.; Xiong, Y.; Zhang, C. π−π Stacking contributing to the low or reduced impact sensitivity of energetic materials. *Cryst. Growth Des.* **2020**, *20*, 2824−2841.

(9) (a) Zhang, C.; Cheng, J.; Wu, Q.; Hou, S.; Feng, S.; Jiang, B.; Lambert, C. J.; Gao, X.; Li, Y.; Li, J. Enhanced π−π stacking between dipole-bearing single molecules revealed by conductance measurement. *J. Am. Chem. Soc.* **2023**, *145*, 1617−1630. (b) Wang, Y.; Hu, L.; Staples, R. J.; Pang, S.; Shreeve, J. M. Highly selective nitroamino isomerization guided by proton transport dynamics: Full-nitroamino imidazole[4,5-d]pyridazine fused-ring system. *ACS Appl. Mater. Interfaces* **2022**, *14*, 52971−52978. (c) Dharmarwardana, M.; Otten, B. M.; Ghimire, M. M.; Arimilli, B. S.; Williams, C. M.; Boateng, S.; Lu, Z.; McCandless, G. T.; Gassensmith, J. J.; Omary, M. A. Strong π-stacking causes unusually large anisotropic thermal expansion and thermochromism. *Proc. Natl. Acad. Sci. U. S. A.* **2021**, *118*, No. e2106572118.

(10) Donoshita, M.; Yoshida, Y.; Hayashi, M.; Ikeda, R.; Tanaka, S.; Yamamura, Y.; Saito, K.; Kawaguchi, S.; Sugimoto, K.; Kitagawa, H. Various stacking patterns of two-dimensional molecular assemblies in hydrogen-bonded cocrystals: Insight into competitive intermolecular interactions and control of stacking patterns. *Angew. Chem., Int. Ed.* **2021**, *60*, 22839−22848.

(11) Breault, G. A.; Hunter, C. A.; Mayers, P. C. Influence of solvent on aromatic interactions in metal tris-bipyridine complexes. *J. Am. Chem. Soc.* **1998**, *120*, 3402−3410.

(12) (a) Liu, Y.; Liu, K.; Wang, Z.; Zhang, X. Host-enhanced π−π interaction for water-soluble supramolecular polymerization. *Chem. − Eur. J.* **2011**, *17*, 9930−9935. (b) Kohmoto, S.; Tsuyuki, R.; Hara, Y.; Kaji, A.; Takahashi, M.; Kishikawa, K. Dual-mode of assembly of anthracene-based imidazolium salts both in non-polar organic solvents and in aqueous solution. *Chem. Commun.* **2011**, *47*, 9158−9160.

(13) (a) Rashkin, M. J.; Waters, M. L. Unexpected substituent effects in offset π−π stacked interactions in water. *J. Am. Chem. Soc.* **2002**, *124*, 1860−1861. (b) Cho, H. J.; Kim, S. W.; Kim, S.; Lee, S.; Lee, J.; Cho, Y.; Lee, Y.; Lee, T.-W.; Shin, H.-J.; Song, C. Suppressing π−π stacking interactions for enhanced solid-state emission of flat aromatic molecules via edge functionalization with picket-fence-type groups. *J. Mater. Chem. C* **2020**, *8*, 17289−17296. (c) Chen, Z.-Y.; Hong, Q.-L.; Zhang, H.-X.; Zhang, J. Induction of chirality in boron imidazolate frameworks: the structure-directing effects of substituents. *Inorg. Chem.* **2022**, *61*, 6861−6868.

(14) Roy, B.; Reddy, M. C.; Hazra, P. Developing the structure−property relationship to design solid state multi-stimuli responsive materials and their potential applications in different fields. *Chem. Sci.* **2018**, *9*, 3592−3606.

(15) (a) Yao, Z.-F.; Wang, J.-Y.; Pei, J. Control of π−π stacking via crystal engineering in organic conjugated small molecule crystals. *Cryst. Growth Des.* **2018**, *18*, 7−15. (b) Moret, M.; Gavezzotti, A. The

crystalline state of rubrene materials: intermolecular recognition, isomorphism, polymorphism, and periodic bond-chain analysis of morphologies. *New J. Chem.* **2022**, *46*, 7626−7637. (c) Fukushima, T.; Sakamoto, H.; Tanaka, K.; Hijikata, Y.; Irle, S.; Itami, K. Polymorphism of [6]cycloparaphenylene for packing structure-dependent host-guest interaction. *Chem. Lett.* **2017**, *46*, 855−857. (d) Lu, C.; Wei, Y.; Zhu, E.; Reutt-Robey, J. E.; Xu, B. Polymorphism in self-assembled structures of 9-anthracene carboxylic acid on Ag (111). *Int. J. Mol. Sci.* **2012**, *13*, 6836−6848. (e) Park, I.-H.; Dey, A.; Sasaki, K.; Ohba, M.; Lee, S. S.; Vittal, J. J. Disappeared supramolecular isomer reappears with perylene guest. *IUCrJ* **2020**, *7*, 324−330.

(16) (a) Yoshizawa, M.; Klosterman, J. K. Molecular architectures of multi-anthracene assemblies. *Chem. Soc. Rev.* **2014**, *43*, 1885−1898. (b) Camposeo, A.; Granger, D. B.; Parkin, S. R.; Altamura, D.; Giannini, C.; Anthony, J. E.; Pisignano, D. Directed functionalization tailors the polarized emission and waveguiding properties of anthracene-based molecular crystals. *Chem. Mater.* **2019**, *31*, 1775−1783. (c) Chiarucci, M.; Mazzanti, A.; Righi, P.; Bencivenni, G.; Mancinelli, M. Noncovalent interactions between stacked arenes in 1,8-bis-(1-naphthyl)-naphthalenes. *Eur. J. Org. Chem.* **2021**, 2594−2603. (d) Sasaki, H.; Wakayama, Y.; Chikyow, T.; Barrena, E.; Dosch, H.; Kobayashi, K. Growth of anthracene derivative thin films with a π-stacking structure. *Appl. Phys. Lett.* **2006**, *88*, No. 081907. (e) Li, Y.; Rajasree, S. S.; Lee, G. Y.; Yu, J.; Tang, J.-H.; Ni, R.; Li, G.; Houk, K. N.; Deria, P.; Stang, P. J. Anthracene-triphenylamine-based platinum(II) metallacages as synthetic light-harvesting assembly. *J. Am. Chem. Soc.* **2021**, *143*, 2908−2919.

(17) Kobayashi, K.; Masu, H.; Shuto, A.; Yamaguchi, K. Control of face-to-face π−π stacked packing arrangement of anthracene rings via chalcogen-chalcogen, Interaction: 9,10-bis(methylchalcogeno)-anthracenes. *Chem. Mater.* **2005**, *17*, 6666−6673.

(18) Chen, R. T. C.; Sun, Y.; Zhao, Y.; Linden, V.; Tuo, W.; Zhang, F.; Zhang, S.; Sepehrpour, H.; Yan, C.; Wang, J.; Li, D.; Stang, P. J. Anthracene-induced formation of highly twisted metallacycle and its crystal structure and tunable assembly behaviors. *Proc. Natl. Acad. Sci. U. S. A.* **2021**, *118*, No. e2102602118.

(19) (a) Wang, C.; Dong, H.; Li, H.; Zhao, H.; Meng, Q.; Hu, W. Dibenzothiophene derivatives: from Herringbone to lamellar packing motif. *Cryst. Growth Des.* **2010**, *10*, 4155−4160. (b) Salini, P. S.; Rajagopal, S. K.; Hariharan, M. Haloacetylation-driven ransformation of sandwich Herringbone to lamellar/columnar packing in pyrene. *Cryst. Growth Des.* **2016**, *16*, 5822−5830. (c) Fujikawa, T.; Segawa, Y.; Itami, K. Synthesis, structures, and properties of π-extended double helicene: a combination of planar and nonplanar π-systems. *J. Am. Chem. Soc.* **2015**, *137*, 7763−7768. (d) Shrestha, B. B.; Higashibayashi, S.; Sakurai, H. Columnar/herringbone dual crystal packing of pyrenylsumanene and its photophysical properties. *Beilstein J. Org. Chem.* **2014**, *10*, 841−847.

(20) Wight, C. D.; Xiao, Q.; Wagner, H. R.; Hernandez, E. A.; Martin, E.; Lynch, V. M.; Iverson, B. L. Properties in symmetric and asymmetric monoalkoxynaphthalene−naphthalimide donor−acceptor dyads influence of the alkyl side chain length on the assembly and thermochromic solid-state. *Cryst. Growth Des.* **2022**, *22*, 7363−7373.

(21) Singh, A. P.; Baruah, J. B. Arrangements among the fluorophores in the salts of imidazole tethered anthracene derivative with pyridinedicarboxylic acids influencing photo-luminescence. *Mater. Adv.* **2022**, *3*, 3513.

(22) Steed, K. M.; Steed, J. W. Packing problems: high Z′ crystal structures and their relationship to cocrystals, inclusion compounds, and polymorphism. *Chem. Rev.* **2015**, *115*, 2895−2933.

(23) (a) Tarai, A.; Baruah, J. B. Separation or union of Non-covalently linked partners provide polymorphs of N-(Aryl)-2-(propan-2-ylidene) hydrazine carbothioamides. *CrystEngComm* **2019**, *21*, 1397−1406. (b) Sendh, J.; Baruah, J. B. Polymorphs, ionic cocrystal and inclusion complex of N-amino-1,8-naphthalimide. *CrystEngComm* **2023**, *25*, 1928−1940.

(24) MacDonald, J. C.; Dorrestein, P. C.; Pilley, M. M.; Foote, M. M.; Lundburg, J. L.; Henning, R. W.; Schultz, A. J.; Manson, J. L. Design of layered crystalline materials using coordination chemistry and hydrogen bonds. *J. Am. Chem. Soc.* **2000**, *122*, 11692−11702.

(25) Shankar, K.; Kirillov, A.; Baruah, J. B. A modular approach for molecular recognition by zinc dipicolinate complexes. *Dalton Trans.* **2015**, *44*, 14411−14423.

(26) Sredojević, D. N.; Tomić, Z. D.; Zarić, S. D. Evidence of chelate-chelate stacking interactions in crystal structures of transition-metal complexes. *Cryst.Growth Des.* **2010**, *10*, 3901−3908.

(27) Gholivand, K.; Hosseini, M.; Valmoozi, A. A. E.; Farshadfar, K. Polymorphism, pseudo-polymorphism, and conformerism in the crystal structure of piperazine-N,N′-bis(N,O-diphenyl phosphoramidate). *CrystEngComm* **2017**, *19*, 2536−2548.

(28) (a) Chen, L.; Berry, S. N.; Wu, X.; Howe, E. N. W.; Gale, P. A. Advances in anion receptor chemistry. *Chem* **2020**, *6*, 61−141. (b) Barboiu, M. Encapsulation versus self-aggregation toward highly selective artificial K⁺ channels. *Acc. Chem. Res.* **2018**, *51*, 2711−2718.

(29) Nichols, G. *Sedimentology and stratigraphy*, 2nd ed.; John Wiley and Sons, 2009; p. 168.

(30) Talukdar, P.; Bollot, G.; Mareda, J.; Sakai, N.; Matile, S. J. Synthetic ion channels with rigid-rod π-stack architecture that open in response to charge-transfer complex formation. *J. Am. Chem. Soc.* **2005**, *127*, 6528−6529.

(31) (a) Braun, D. E.; Schneeberger, A.; Griesser, U. J. Understanding the role of water in 1,10-phenanthroline monohydrate. *CrystEngComm* **2017**, *19*, 6133−6145. (b) Baruah, J. B.; Karmakar, A.; Barooah, N. Solvent induced symmetry non-equivalence in crystal lattice of 7-carboxymethyl-1,3,6,8-tetraoxo-3,6,7,8-tetrahydro-1H-benzo[lmn]-[3,8]phenathrolin-2-yl acetic acid. *CrystEngComm* **2008**, *10*, 151−154.

(32) (a) Butler, C. J.; Yoshida, M.; Hanaguri, T.; Iwasa, Y. Mottness versus unit cell doubling as the driver of the insulating state in 1T-TaS₂. *Nat. Commun.* **2020**, *11*, 2477. (b) Andrault, D.; Fiquet, G.; Kunz, M.; Visocekas, F.; Hausermann, D. The orthorhombic structure of iron: an in situ study at high-temperature and hgh-pressure. *Science* **1997**, *278*, 831−834. (c) Edkins, K.; McIntyre, G. J.; Wilkinson, C.; Kahlenberg, V.; Toobbens, D.; Griesser, U. J.; Bruning, J.; Schmidt, M. U.; Steed, J. W. Extensive sequential polymorphic interconversion in the solid state: two hydrates and ten anhydrous phases of hexamidine diisethionate. *Cryst. Growth Des.* **2019**, *19*, 7280−7289. (d) Nath, J.; Baruah, J. B. Self-assemblies of solvates, Ionic cocrystals, and a salt based on 4-{[(4-nitrophenyl)carbamoyl]amino}-N-(pyrimidin-2-yl)benzene-1-sulfona-mide: study in the solid and solution states. *Cryst. Growth Des.* **2021**, *21*, 5325−5341.

(33) Peebles, C.; Alvey, P. M.; Lynch, V.; Iverson, B. L. Time-dependent solid-state polymorphism of a series of donor−acceptor dyads. *Cryst. Growth Des.* **2014**, *14*, 290−299.

(34) Inoue, S.; Nikaido, K. I.; Higashino, T.; Arai, S.; Tanaka, M.; Kumai, R.; Tsuzuki, S.; Horiuchi, S.; Sugiyama, H.; Segawa, Y.; Takaba, K.; Maki-Yonekura, S.; Yonekura, K.; Hasegawa, T. Emerging disordered layered-Herringbone phase in organic semiconductors unveiled by electron crystallography. *Chem. Mater.* **2022**, *34*, 72−83.

(35) Abe, Y.; Savikhin, V.; Yin, J.; Grimsdale, A. C.; Soci, C.; Toney, M. F.; Lam, Y. M. Unique reversible crystal-to-crystal phase transition structural and functional properties of fused ladder thienoarenes. *Chem. Mater.* **2017**, *29*, 7686−7696.

(36) Zhou, L.; Yin, Q.; Du, S.; Hao, H.; Li, Y.; Liu, M.; Hou, B. Crystal structure, thermal crystal form transformation, desolvation process and desolvation kinetics of two novel solvates of ciclesonide. *RSC Adv.* **2016**, *6*, 51037−51045.

(37) Nath, J.; Kirillov, A.; Baruah, J. B. Unusual solvent-mediated hydrolysis of dicarboxylate monoester ligands in copper(II) complexes toward simultaneous crystallization of new dicarboxylate derivatives. *RSC Adv.* **2014**, *4*, 47876−47886.